Arrested Chain Growth During Magnetic Directed Particle Assembly in Yield Stress Matrix Fluids

Jason P. Rich[1], *Gareth H. McKinley*[2]*, *and Patrick S. Doyle*[1]*

[1]Department of Chemical Engineering, Massachusetts Institute of Technology, Cambridge MA 02139

[2]Hatsopoulos Microfluids Laboratory, Department of Mechanical Engineering, Massachusetts Institute of Technology, Cambridge MA 02139

*pdoyle@mit.edu, gareth@mit.edu

RECEIVED DATE (to be automatically inserted after your manuscript is accepted if required according to the journal that you are submitting your paper to)

Title Running Head: Magnetic Directed Assembly in Yield Stress Fluids

(P.S.D.) Tel: +1-617-253-4534. Fax: +1-617-324-0066. (G.H.M.) Tel: +1-617-258-0754. Fax: +1-617-258-8559.

Abstract

The process of assembling particles into organized functional structures is influenced by the rheological properties of the matrix fluid in which the assembly takes place. Therefore, tuning these properties represents a viable and as yet unexplored approach for controlling particle assembly. In this letter, we examine the effect of the matrix fluid yield stress on the directed assembly of polarizable particles into linear chains under a uniform external magnetic field. Using particle-level simulations with a simple yield stress model, we find that chain-growth follows the same trajectory as in Newtonian matrix fluids up to a critical time that depends on the balance between the yield stress and the strength of magnetic

interactions between particles; subsequently, the system undergoes structural arrest. Appropriate dimensionless groups for characterizing the arresting behavior are determined and relationships between these groups and the resulting structural properties are presented. Since field-induced structures can be indefinitely stabilized by the matrix fluid yield stress and 'frozen' into place as desired, this approach may facilitate the assembly of more complex and sophisticated structures.

Keywords: directed assembly, yield stress, structural arrest, dipolar chains, magnetorheological fluids

1. Introduction

The assembly of colloids and nanoparticles into complex and highly-ordered structures continues to be an important and effective method for creating functional materials with unique and technologically attractive properties.[1,2] Through manipulation of the thermodynamic and kinetic interactions between particle building blocks, authors have demonstrated the assembly of materials such as photonic crystals[3] and electronic circuits,[4,5] as well as biomaterials such as peptide-based scaffolds for regenerative medicine.[6,7] Approaches to controlling the assembly process generally fall into three categories: adjusting particle or template properties like shape, size, patterning, and chemical functionality;[8,9] tuning particle interactions via thermodynamic variables such as temperature or pH;[10,11] and directing particle behavior with external flows or fields, such as electric or magnetic fields.[2,12] In particular, by applying a uniform magnetic field to polarizable colloids suspended in a matrix fluid, directed assembly of the particles into aggregated chain-like structures in the direction of the external field can be achieved.[13] The anisotropic mechanical properties of these structures have been exploited in magnetorheological (MR) fluids,[14,15] which undergo dramatic changes in bulk rheological properties upon formation of particle chains, as well as for lab-on-a-chip separations.[16] The matrix fluid in most particle assembly studies, as well as in most MR fluids and devices, is typically Newtonian; however, it has long been known in the rheology community that the behavior of suspended particles is significantly influenced by the matrix fluid rheology.[17] For example, Feng and Joseph demonstrated that spherical particles dispersed in viscoelastic Boger fluids subjected to bulk torsional flow undergo radial migration to form distinct ring patterns; by contrast, no such microstructure was observed in the Newtonian case.[18] Additionally, the use of yield stress matrix fluids to prevent sedimentation in MR suspensions has motivated questions about the effects of the yield stress on the formation of field-induced structures.[19,20]

With these considerations in mind, we present in this letter a new approach to controlling particle assembly via the non-Newtonian properties of the matrix fluid. Because of the immediate relevance to MR fluid technology, we specifically demonstrate this approach by examining the effect of the matrix fluid yield stress on the directed assembly of polarizable particles under a uniform external

magnetic field. Using 2-D particle-level simulations, we find that chain growth initially follows the same trajectory as in Newtonian matrix fluids, but is arrested at a critical time that scales with a dimensionless group that characterizes the balance between the yield stress and inter-particle magnetic stresses. Adjusting this balance allows the properties of the arrested structure, including the average cluster size, to be tuned. Assuming the matrix fluid yield stress dominates over other forces on particles (i.e., thermal, gravitational, electrostatic, etc.), arrested structures are indefinitely stable even after the magnetic field is removed, being essentially 'frozen' in the matrix until additional manipulation is desired. This behavior is generic to particle dynamics in yield stress matrix fluids and could be exploited in other types of assembly processes, including assembly via electric fields, fluid flow, or chemical interactions. Finally, this letter will have important implications for the formulation and understanding of MR suspensions stabilized by yield stress matrix fluids. We identify regimes in which the arrest of dipolar chain-formation due to the matrix fluid yield stress is expected to significantly impact the field-induced rheological properties.

2. Simulation Details

The simulation method used in this work is adopted from a previously described algorithm,[21,22] which was developed to study field-induced chaining of dipolar particle suspensions in Newtonian matrix fluids. We review the essential features of this method and discuss the modifications necessary to incorporate a matrix fluid yield stress. The pair-wise magnetic interaction energy U_{ij}^{mag} between two dipoles separated by a distance r_{ij} is given by:

$$U_{ij}^{mag} = \frac{m^2 \mu_0}{4\pi}\left(\frac{1-3\cos\theta_{ij}}{r_{ij}}\right) \tag{1}$$

Here $m = |\mathbf{m}|$ is the magnitude of the dipole moment, μ_0 is the magnetic permeability of the medium (assumed to be equal to the permeability of free space), and θ_{ij} is the angle that the line connecting the particle centers makes with the direction of the applied magnetic field. Though eq 1 neglects mutual magnetic induction and treats particles as point dipoles with identical dipole moments aligned with the external magnetic field, this expression has been successful in quantitatively capturing the particle-level behavior in MR suspensions subject to a uniform external magnetic field,[21,23,24] providing results consistent with experimental observations.[25] In the work of Haghgooie,[22] the Heyes–Melrose displacement algorithm is used to correct for hard-sphere overlaps between dipolar particles at each time step of the simulation.[26] This approach complicates the incorporation of a matrix fluid yield stress,

however, because it accounts for excluded volume interactions through a constraint rather than an explicit potential. Additionally, we find that when attempts are made to incorporate a matrix fluid yield stress, the Heyes–Melrose algorithm leads to unphysical behavior such as 'kinked' chains that drift in a direction perpendicular to the applied magnetic field. Therefore, we instead include a short-ranged repulsive potential between particles:[27]

$$U_{ij}^{rep} = \frac{3\mu_0 r_c m^2}{4\pi d^4} \exp\left(-\frac{r_{ij} - d}{r_c}\right) \tag{2}$$

where d is the particle diameter, and r_c is a constant that controls the range of the interaction. For our work, we set $r_c = 0.05d$. Lower values of r_c better approximate a hard-sphere potential, but require prohibitively short time steps. The pre-exponential factor, including its dependence on m and μ_0, ensures that the magnetic and excluded volume interactions are of a similar order of magnitude for particle separations on the order of r_c, resulting in stable simulations that approximate the behavior of hard-sphere magnetic particles. In order to simplify the simulation so that effects of the matrix fluid yield stress can be more easily distinguished, we neglect thermal forces and hydrodynamic interactions. In this case, the total force $\mathbf{F}_i$ on particle i at time t is calculated as:

$$\mathbf{F}_i(t) = \sum_{i \neq j}^{N} -\nabla\left[U_{ij}^{mag}\left(r_{ij}(t), \theta_{ij}(t)\right) + U_{ij}^{rep}\left(r_{ij}(t)\right)\right] \tag{3}$$

The Langevin equation describing the particle velocity is then

$$d\mathbf{r}_i(t) ; \frac{1}{\zeta}\mathbf{F}_i(t)dt \tag{4}$$

where ζ is the drag coefficient of a particle. Eq 4 therefore represents a balance between magnetic, excluded volume, and drag forces on a particle. In order to generalize the simulation results, eq 4 is made dimensionless using the characteristic length scale d and the characteristic force $F_{char} = \pi d^2 \mu_0 (\rho M)^2 / 24$, where ϱ is the particle mass density, and M is the particle magnetization per unit mass. M is related to the dipole moment m via the expression $M = m/V\rho$, where V is the volume of a particle. F_{char} represents the force between two particles aligned with the field and in contact. Applying these scalings, the dimensionless Langevin equation becomes

$$d\hat{\mathbf{r}}_i\left(\hat{t}\right);\ \hat{\mathbf{F}}_i\left(\hat{t}\right)d\hat{t} \tag{5}$$

where $\hat{}$ represents dimensionless variables. Setting $t_{char} = 24\zeta/\pi d\mu_0\left(\rho M\right)^2$ as the characteristic time scale removes all free parameters from the dimensionless Langevin equation. This time scale represents the time necessary for a particle to move a distance of one particle diameter in response to the characteristic driving force F_{char}.

A Bingham viscoplastic model for a yield stress matrix fluid is incorporated by applying a constraint to eq 5. We make the simple approximation that a particle moves during a time step only if the sum of the forces on the particle (including both magnetic and short-range steric forces) is sufficient to overcome the matrix fluid yield stress, τ_y. Otherwise, the particle remains motionless for that time step. Mathematically, if $\left\|\mathbf{F}_i\right\| \geq \pi d^2\tau_y/2C$, then the particle executes a step according to eq 5; otherwise, $d\hat{\mathbf{r}}_i$ is set to 0. C is a constant that relates the matrix fluid yield stress to the critical force necessary to cause an embedded particle to yield. For spherical particles in Bingham fluids, Beris *et al*. showed using finite-element modeling that $C \approx 0.143$.[28] In dimensionless terms, the criteria for yielding is

$$\left\|\hat{\mathbf{F}}_i\right\| \geq \frac{12\tau_y}{\mu_0 C\left(\rho M\right)^2} = \frac{1}{\mathrm{Y}_{\mathrm{M}}^*} \tag{6}$$

$$\mathrm{Y}_{\mathrm{M}}^* \equiv \frac{\mu_0 C\left(\rho M\right)^2}{12\tau_y} \tag{7}$$

The dimensionless yield parameter $\mathrm{Y}_{\mathrm{M}}^*$ can be understood as the characteristic inter-particle magnetic stress divided by the matrix fluid yield stress τ_y. That is, for $\mathrm{Y}_{\mathrm{M}}^* ?\ 1$, magnetic forces dominate over the yield stress, while $\mathrm{Y}_{\mathrm{M}}^* = 1$ corresponds to an immobilized system in which magnetic forces are too weak to overcome the yield stress. Note that this dimensionless group is similar to the so-called "magnetic yield parameter" introduced by previous authors.[19]

Simulations are conducted in 2-D with a uniform external magnetic field in the vertical direction. The simulation box is square with a side length equal to 100 particle diameters and periodic boundary conditions on all sides. To begin simulations, particles are initially placed in the box in a random configuration with no particle overlaps and eq 5 is integrated forward in time using a simple

Euler scheme for 1000 time steps at a time-step size of $\Delta\hat{t} = 3.3\times10^{-7}$. The purpose of this short preparatory simulation using a very small time step is to resolve the trajectories of any particles positioned very close to each other in the random initial placements. Subsequently, the time-step size is increased to $\Delta\hat{t} = 3.3\times10^{-4}$ for the remainder of the simulation. The constraint in eq 6 is applied at each time step. A dimensionless spatial cutoff (scaled with the particle diameter) for the inter-particle forces of 15 was used along with a linked-list binning algorithm with bin sizes that slightly exceed the cutoff value.[21,22,29] Interested readers are referred to earlier communications for additional details about the simulation algorithm.[21,22]

3. Results and Discussion

It is well-known that applying a uniform magnetic field to a dispersion of polarizable spherical particles in a Newtonian matrix fluid results in the formation of long-chain structures in the direction of the external field. Since a matrix fluid with a strong enough yield stress will completely immobilize particles, we examine magnetic directed assembly in a regime where both magnetic interactions and the matrix fluid yield stress play an important role in structure formation. Because the characteristic force in our simulations is defined as the maximum force between two dipolar particles, the regime of interest corresponds to values $\mathrm{Y}_{\mathrm{M}}^{*} > 1$.

Images of magnetically assembled structures after long times $\left(\hat{t} = 2667\right)$ are shown in Figure 1 for dispersions with a particle area fraction of $\phi_A = 0.15$ and magnetic yield parameters of (A) $\mathrm{Y}_{\mathrm{M}}^{*} = 6.7$, (B) $\mathrm{Y}_{\mathrm{M}}^{*} = 67$, and (C) the Newtonian case $\left(\mathrm{Y}_{\mathrm{M}}^{*} \to \infty\right)$. At $\mathrm{Y}_{\mathrm{M}}^{*} = 6.7$, only a marginal development of the structure from the initial condition is observed, as the arrested configuration consists of a randomly distributed mixture of individual particles and small chains; the magnetic interactions are not strong enough to generate large-scale structures. At $\mathrm{Y}_{\mathrm{M}}^{*} = 67$, the average chain length is significantly longer in the arrested state, and the vast majority of particles are incorporated in vertically-aligned chains. As $\mathrm{Y}_{\mathrm{M}}^{*}$ increases, the limiting Newtonian case is approached, for which domain-spanning chains are formed and some lateral aggregation of chains is evident. We note that while (A) and (B) represent arrested configurations, chaining and lateral aggregation continue very slowly in the Newtonian system even up to $\hat{t} = 2667$. See the supporting information included with this article for movies of magnetic directed assembly at $\phi_A = 0.15$ and various values of $\mathrm{Y}_{\mathrm{M}}^{*}$.

As a first step towards understanding this behavior, we consider a simpler system of two dipolar particles in a yield stress matrix fluid. With one particle fixed at the origin, yielding occurs if the

distance to the second particle is sufficiently small that the inter-particle force overcomes the matrix fluid yield stress; otherwise, both particles remain immobile. For this system, the critical positions for yielding can be found by solving for the contour on which the magnitude of the dimensionless force on the second particle is equal to $1/\mathrm{Y}_{\mathrm{M}}^{*}$, as in the yield criteria in eq 6. Neglecting the repulsive steric force, which is much smaller than the magnetic force for these inter-particle distances, the magnitude of the force on the particle is calculated from eqs 1 and 3:

$$\left\|\mathbf{F}_i\right\| \approx \left\|-\nabla U_{ij}^{mag}\left(r_{ij},\theta_{ij}\right)\right\| = \sqrt{\left(\frac{\partial U_{ij}^{mag}}{\partial r_{ij}}\right)^2 + \frac{1}{r_{ij}^2}\left(\frac{\partial U_{ij}^{mag}}{\partial \theta_{ij}}\right)^2} = \frac{3m^2\mu_0}{4\pi r_{ij}^4}\sqrt{\left(1-3\cos^2\theta_{ij}\right)^2 + \sin^2\left(2\theta_{ij}\right)} \qquad (8)$$

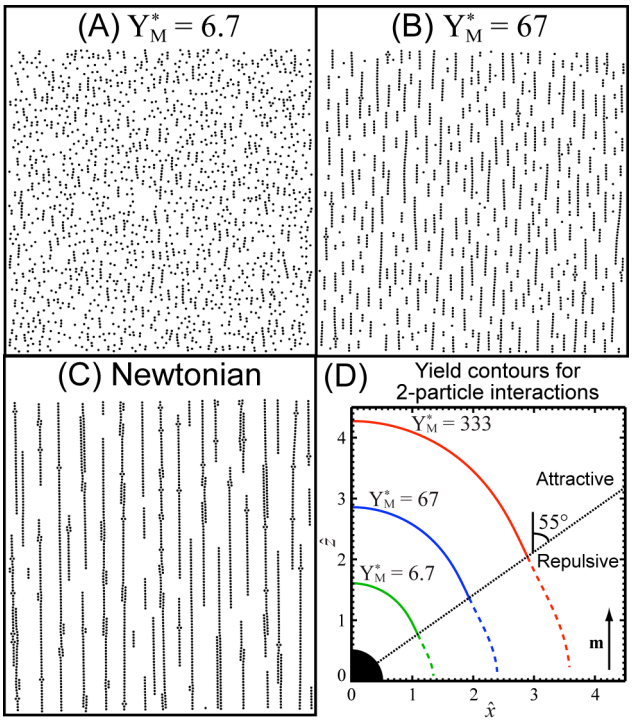

Figure 1. Magnetically assembled structures at $\phi_A = 0.15$ at long times $\left(\hat{t} = 2667\right)$ for dimensionless magnetic yield parameters of (A) $\mathrm{Y}_{\mathrm{M}}^{*} = 6.7$ and (B) $\mathrm{Y}_{\mathrm{M}}^{*} = 67$, and (C) the Newtonian case $\left(\mathrm{Y}_{\mathrm{M}}^{*} \to \infty\right)$. The applied magnetic field is in the vertical direction. While a mixture of individual particles and short chains is observed at $\mathrm{Y}_{\mathrm{M}}^{*} = 6.7$, increasing $\mathrm{Y}_{\mathrm{M}}^{*}$ results in an arrested state with greater numbers of particles incorporated into longer chains. In (D), contours show the critical configurations at which yielding occurs in a 2-particle system at various values of $\mathrm{Y}_{\mathrm{M}}^{*}$. With one particle fixed at the origin, a second particle yields if its position is on or inside the contour (given by eq 10); otherwise, the system is arrested. Depending on the angle between the line connecting the particle centers and the direction of

the dipole moment **m**, magnetic interactions are attractive or repulsive. The yield contours expand with Y_M^* and are symmetric across the vertical and horizontal axes.

The magnitude of the dimensionless force is therefore

$$\left\|\hat{\mathbf{F}}_i\right\| \approx \frac{1}{2\hat{r}_{ij}^4}\sqrt{\left(1-3\cos^2\theta_{ij}\right)^2+\sin^2\left(2\theta_{ij}\right)} \tag{9}$$

Setting $\left\|\hat{\mathbf{F}}_i\right\| = 1/Y_M^*$ gives the expression for the yield contour.

$$\hat{r}_{ij}\left(\theta_{ij}\right) \approx \left[\frac{Y_M^*}{2}\sqrt{\left(1-3\cos^2\theta_{ij}\right)^2+\sin^2\left(2\theta_{ij}\right)}\right]^{1/4} \tag{10}$$

Contours corresponding to eq 10 are plotted in Figure 1(D) for identical vertically-directed dipole moments **m** and Y_M^* values of 6.7, 67, and 333. As Y_M^* increases, the contours expand and particles positioned farther from the origin are able to yield in response to the applied magnetic field. Because of the angular dependence of dipolar interactions, the inter-particle force is either attractive ($0° \le \theta_{ij} < 55°$, solid lines), for which yielded particles undergo aggregation, or repulsive ($55° < \theta_{ij} \le 90°$, dotted lines), for which particles tend towards an unaggregated arrested state. Though only one quadrant is shown in Figure 1(D), the contours are symmetric across the vertical and horizontal axes. While multi-particle interactions captured in the full simulations (including the behavior of particle chains) are more complex than this two-particle system, the contours in Figure 1(D) are nonetheless helpful in understanding the basic physical phenomena underlying dipolar particle suspensions in the presence of a yield stress. In particular, Figure 1(D) implies that a particle (or a chain of particles) is arrested when the envelope defined by the yield contour becomes devoid of particles. By extension, the entire system becomes arrested when all distances between distinct clusters fall outside of the yield contours that result from the summation of all inter-particle interactions.

The images in Figure 1 imply that the magnetically assembled structures consist primarily of vertically-connected, chain-like aggregates, and that a relatively small amount of lateral aggregation can occur at higher values of Y_M^*. To explore the directionality of structures quantitatively, we calculate the

vertical connectivity, C_v, and the horizontal connectivity, C_h, defined as the number of vertical and horizontal connections, respectively, scaled by $N - 1$, where N is the number of particles in the simulation.[22] One connection is counted for each pair of particles with centers separated by a dimensionless distance of at most 1.05 (i.e., the radii at contact + 5%). Connections are considered to be vertical if $\theta_{ij} \leq 30°$ or $\theta_{ij} \geq 150°$, and horizontal if $30° < \theta_{ij} < 150°$. The vertical and horizontal connectivities C_v and C_h, respectively, are plotted in Figure 2 as functions of the dimensionless time for various values of $\mathrm{Y}_{\mathrm{M}}^{*}$, with the top curves representing C_v and the bottom curves representing C_h. All simulations begin with the same initial condition of randomly placed particles. The vertical connectivity C_v generally grows with time and, after an initial rearrangement of the starting configuration, is at least an order of magnitude greater than C_h for all $\mathrm{Y}_{\mathrm{M}}^{*}$. These observations are consistent with the formation of vertically-aligned chains as shown in Figure 1. The horizontal connectivity C_h decreases during the initial rearrangement, exhibiting some scatter due to very small numbers of horizontal connections, then increases as some lateral aggregation of chains occurs on longer time scales. Perhaps the most striking feature of the results is that at a critical time (which increases with $\mathrm{Y}_{\mathrm{M}}^{*}$) both connectivity measures diverge from the common trajectory that coincides with the behavior of the Newtonian system. Subsequent to this separation, both C_v and C_h plateau and cease to evolve in the systems with a yield stress matrix fluid. Movies of the particle behavior (see supporting information) confirm that all particles are immobilized when the plateau in the connectivity data is attained. This behavior implies that while the matrix fluid yield stress does not affect the mechanism of structural development, it results in an arrest of chain growth. Though it is reasonable to expect that a matrix fluid yield stress would hinder structure formation, it is remarkable that the dynamics for all $\mathrm{Y}_{\mathrm{M}}^{*}$ values appear to follow the Newtonian trajectory until a critical time corresponding to the onset of structural arrest.

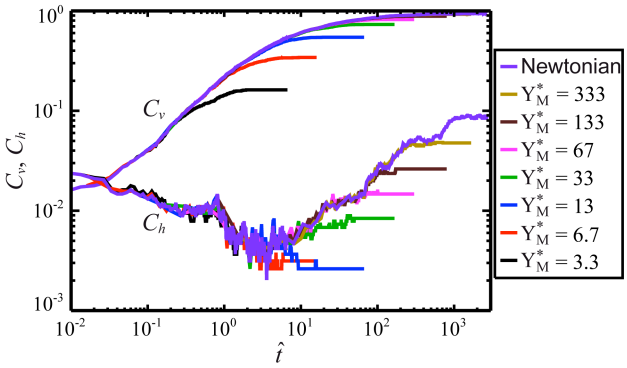

Figure 2. Time evolution of the vertical and horizontal connectivities (C_v and C_h, respectively) of magnetically assembled anisotropic chain structures for a system at $\phi_A = 0.15$ and various values of $\mathrm{Y}_{\mathrm{M}}^{*}$.

All simulations begin with the same initial condition of randomly placed particles. With the exception of an initial decline in C_h during rearrangement of the starting configuration, the connectivities generally grow with time, following the Newtonian result until deviations begin at a critical time and connectivity that increase with $\mathrm{Y}_{\mathrm{M}}^{*}$. The fact that C_v ? C_h after the initial rearrangement indicates that chains are primarily vertically connected, as is seen in Figure 1.

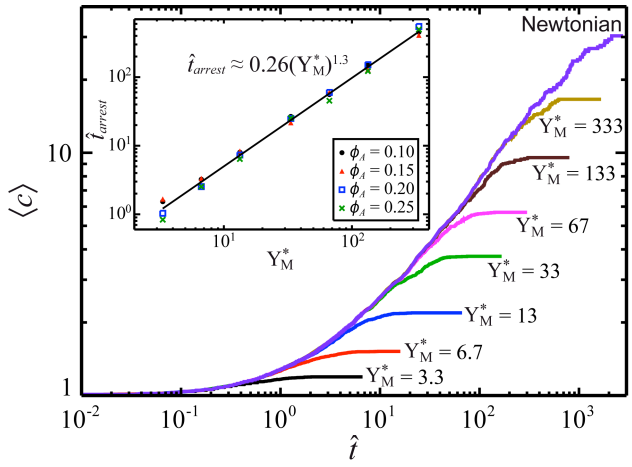

Figure 3. Average cluster size $\langle c \rangle$ of magnetically assembled structures as a function of time for various values of $\mathrm{Y}_{\mathrm{M}}^{*}$. The data is extracted from the same simulations as in Figure 2, for which $\phi_A = 0.15$. As with the connectivity results, $\langle c \rangle$ generally increases with time, but chain growth is eventually arrested when a yield stress matrix fluid is present. For all values of $\mathrm{Y}_{\mathrm{M}}^{*}$, $\langle c \rangle$ follows a common trajectory until structural arrest begins at a critical time (and a critical cluster size) that grows with $\mathrm{Y}_{\mathrm{M}}^{*}$. The arrest time, $\hat{t}_{arrest}$, defined as the time at which $\langle c \rangle$ becomes less than 90% of the Newtonian case, is shown in the inset as a function of $\mathrm{Y}_{\mathrm{M}}^{*}$. Results for four concentrations collapse onto a single common power law relationship.

The observation that suspensions of dipolar particles in yield stress matrix fluids undergo structural arrest from a common trajectory is also supported by data for the time-evolution of the average cluster size, $\langle c \rangle$, shown in Figure 3 for the same simulation conditions shown in Figure 2. The

average cluster size is calculated as $\langle c \rangle = N/N_c$, where N_c is the total number of clusters and a cluster is identified as a collection of continuously connected particles according to the definition of a connection given above.[22] The average cluster size grows with time and, in accordance with the connectivity results, data at finite values of Y_M^* break away from a common trajectory at a critical time that increases with Y_M^*. Upon reaching structural arrest in the yield stress systems, $\langle c \rangle$ plateaus at values that grow with Y_M^* but are uniformly smaller than the long-time Newtonian result. Taking the critical arrest time, $\hat{t}_{arrest}$, as the time at which $\langle c \rangle$ becomes less than 90% of the Newtonian value, we plot $\hat{t}_{arrest}$ as a function of Y_M^* in the inset of Figure 3 for four different concentrations of magnetic particles. The data follows a power law behavior, and least-squares fitting provides the relationship $\hat{t}_{arrest} \approx 0.26\left(Y_M^*\right)^{1.3}$, which is shown by the black line. The results for all four concentrations collapse onto this function, indicating that the arrest time is approximately independent of area fraction ϕ_A and that Y_M^* is the appropriate dimensionless group for characterizing the dynamics of structural arrest over a range of concentrations.

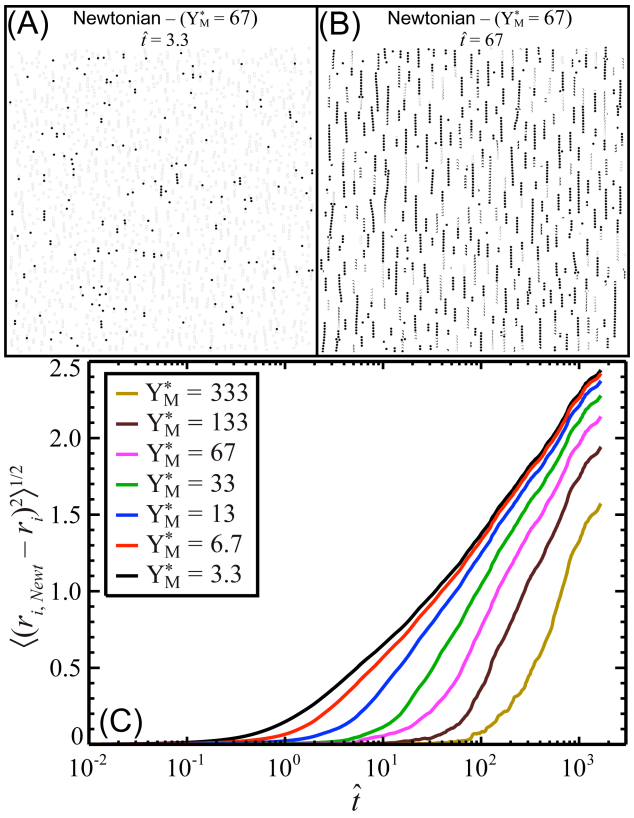

Figure 4. Comparison of the magnetically assembled structures for particle suspensions in Newtonian and yield stress matrix fluids at $\phi_A = 0.15$. An imposed magnetic field in the vertical direction induces a vertically-aligned dipole moment on the particles. For times of (A) $\hat{t} = 3.3$ and (B) $\hat{t} = 67$, images of a Newtonian system are shown in black and images of a yield stress system at $Y_M^* = 67$ are overlaid in

white. Therefore, any visible black structures indicate differences between the two systems. (A) and (B) correspond to times before and just after structural arrest in the yield stress system, respectively. At early times, the structures of the two systems are nearly identical, whereas significant deviations are apparent after the onset of structural arrest. The supporting information provides movies analogous to these overlaid images, as well as a magnified image of (A) that more clearly portrays the particle overlaps. In (C), the ensemble-averaged root mean square difference between particle positions in the Newtonian and yield stress system is plotted as a function of time for various values of $\mathrm{Y}_{\mathrm{M}}^{*}$. This measure of the deviation in the structure from the Newtonian case is essentially zero up to a critical time, then grows once the yield stress systems become arrested.

While the correspondence of statistical quantities like C_v, C_h, and $\langle c \rangle$ between the Newtonian and yield stress systems prior to arrest is a compelling indicator of a common trajectory of structural states, these averaged quantities do not uniquely identify the magnetically assembled structures. To more convincingly demonstrate that systems at finite values of $\mathrm{Y}_{\mathrm{M}}^{*}$ truly pass through the same structural states as the Newtonian system, it is useful to examine the positions of each particle at a given time. A simple and instructive way to compare the positions of many particles simultaneously is to effectively subtract a snapshot of a simulated structure in a yield stress matrix fluid from that of the Newtonian system at the same dimensionless time. This can be accomplished by displaying the structure of the Newtonian system in black, and overlaying the structure of yield stress system in white, so that any visible black regions indicate structures that are not common between the two systems. Such comparisons between structures in a Newtonian matrix fluid and a matrix fluid at $\mathrm{Y}_{\mathrm{M}}^{*} = 67$ (starting from the same initial condition at $\phi_A = 0.15$) are shown in Figure 4 at dimensionless times of (A) $\hat{t} = 3.3$ and (B) $\hat{t} = 67$, corresponding to times before and just after the onset of structural arrest in the yield stress system, respectively (here $\hat{t}_{arrest} = 60$). This effective subtraction of images almost completely obscures the structure at $\hat{t} = 3.3$, suggesting that the magnetically assembled structures of the Newtonian and yield stress systems are essentially the same prior to structural arrest. Note that the light gray outlines indicate that the white particles of the system at $\mathrm{Y}_{\mathrm{M}}^{*} = 67$ are overlaid almost exactly on the black particles of the Newtonian simulation [see supporting information for a magnified image of Figure 4(A)]. At $\hat{t} = 67$, however, there are significant deviations between the two systems, reflecting the fact that while chain-formation continues in the Newtonian system, structural evolution in the yield stress system has slowed almost to a halt. These images are consistent with the behavior presented in

Figures 2 and 3, and support the hypothesis that particles in the Newtonian and yield stress systems follow very similar trajectories up to the critical arrest time $\hat{t}_{arrest}$, after which the yield stress systems are quenched and deviations between the structures in the two systems grow. Movies analogous to the overlaid images in Figures 4(A) and 4(B) are provided as supporting information. The deviations between the Newtonian and yield stress systems can be explored quantitatively by calculating the ensemble-averaged root mean square difference in particle position between the structures in the Newtonian matrix fluid and the yield stress matrix fluid. Denoted $\left\langle \left(r_{i,Newt} - r_i \right)^2 \right\rangle^{1/2}$, this quantity is zero if particles are in the same positions in the two systems, and grows as the structures diverge. Figure 4(C) shows that for all $\mathrm{Y}_{\mathrm{M}}^*$, $\left\langle \left(r_{i,Newt} - r_i \right)^2 \right\rangle^{1/2} \approx 0$ up to a critical time that increases with $\mathrm{Y}_{\mathrm{M}}^*$ and corresponds approximately with the values of $\hat{t}_{arrest}$ shown in the inset of Figure 3. Subsequently, $\left\langle \left(r_{i,Newt} - r_i \right)^2 \right\rangle^{1/2}$ grows with time as the yield stress systems are arrested and structural development continues in the Newtonian system. These results provide further demonstration that the magnetically assembled structures in yield stress matrix fluids closely match those in Newtonian matrix fluids up to a critical time corresponding to the onset of structural arrest in the yield stress systems. See Figure S2 in the supporting information for a plot analogous to Figure 4(C), but with time re-scaled by $\hat{t}_{arrest}$ to demonstrate that the deviations between particle positions develop due to the onset of structural arrest in the yield stress systems.

The results presented thus far have implications in the design of structures generated via directed assembly or self-assembly. While previous approaches to tuning particle assembly have focused on modifying particles (i.e., their shape, size, patterning, or chemical functionality[8]) or employing particle systems that respond to externally applied fields or stimuli,[30] the concept of regulating assembled structures via matrix fluid rheology has yet to be explored. Our simulations suggest that by incorporating a matrix fluid with a yield stress, the chain structures that form in suspensions of dipolar particles in Newtonian matrix fluids can be arrested at essentially any point in their development. If the yield stress is sufficient to suppress sedimentation and Brownian motion, then arrested structures will be 'frozen' into place indefinitely even if the magnetic field is decreased or removed. Increasing the magnetic field (i.e., increasing $\mathrm{Y}_{\mathrm{M}}^*$) leads to the continuation of chain growth, and the resulting long-time value of $\langle c \rangle$ is approximately independent of the exact history as long as it is approached from below. See the supporting information for a figure demonstrating this behavior. In order to confirm the results presented here, it will be necessary to show that experiments corroborate our observations. These

experiments could be accomplished by examining the magnetic directed assembly of monodisperse spherical polymer-based superparamagnetic particles (available from a variety of vendors) in a yield stress matrix fluid. A simple yield stress fluid that exhibits negligible thixotropy, such as a Carbopol 'microgel', would be useful in exploring and demonstrating the basic phenomena of these field-activated suspensions.[31,32] For example, a system at $Y_M^* \approx 67$ could be achieved by suspending 4.5 μm Dynabeads® superparamagnetic particles (Invitrogen, Carlsbad, CA) in a dilute Carbopol microgel with a yield stress of about 0.1 Pa[33] and by applying a uniform magnetic field of about 0.1 T (according to magnetization data provided by the manufacturer).

With the exception of data for the critical arrest time shown in the inset of Figure 3, all the results presented thus far have been at a representative concentration of ϕ_A = 0.15. While systems at different concentrations exhibit qualitatively similar behavior (and, in particular, Figure 3 shows that $\hat{t}_{arrest}$ is approximately independent of concentration), it would be beneficial to identify the scaling relationship between structural parameters and particle concentration. A simple approximation for the effect of particle concentration can be obtained by adjusting the characteristic length scale in the problem to reflect the concentration dependence of the average inter-particle distance in the random initial condition. For a 2-dimensional homogeneous spatial distribution of spherical particles with diameter d, the average inter-particle distance scales according to $d\phi_A^{-1/2}$. The effect of re-defining $d\phi_A^{-1/2}$ as the new characteristic length scale can be seen from the non-dimensionalization and rearrangement of eq 8, for example. With this new scaling, the expression analogous to eq 10 contains the product $Y_M^*\phi_A^2$ rather than simply Y_M^* as in eq 10. This motivates the definition of a re-scaled yield parameter, $Y_{M,\phi}^*$, that incorporates the concentration dependence:

$$Y_{M,\phi}^* = Y_M^*\phi_A^2 = \frac{\mu_0 C(\rho M)^2}{12\tau_y}\phi_A^2 \tag{11}$$

By analogy with the yield parameter Y_M^*, we expect largely immobilized particles for $Y_{M,\phi}^*$ = 1, and extensive chain formation for $Y_{M,\phi}^*$? 1. The average cluster size at structural arrest, $\langle c \rangle_{arrest}$, is shown as a function of $Y_{M,\phi}^*$ in Figure 5 for four particle area fractions. Despite the crude approximations used to arrive at the concentration scaling in eq 11, plotting $\langle c \rangle_{arrest}$ as a function of $Y_{M,\phi}^*$ collapses data at different concentrations over almost two orders of magnitude of $Y_{M,\phi}^*$. For $Y_{M,\phi}^*$ values of about 0.2 to 7, a range in which both the matrix fluid yield stress and magnetic interactions are expected to play

significant roles in the structure and dynamics, $\langle c \rangle_{arrest}$ is given by the expression $\langle c \rangle_{arrest} \approx 4.5\left(Y^*_{M,\phi}\right)^{0.65}$ for $0.10 \le \phi_A \le 0.25$. The collapse of data for different concentrations indicates that eq 11 provides an appropriate scaling for describing the arrested structure in this regime. The scaling breaks down, however, above about $Y^*_{M,\phi} \approx 7$. In this regime, the values of $\langle c \rangle$ at long times approach the Newtonian values and for $Y^*_{M,\phi} \approx 60$ the systems essentially behave as Newtonian. The gray band gives the range of long-time $\langle c \rangle$ values for Newtonian systems with concentrations $0.10 \le \phi_A \le 0.25$, which represents an upper bound for $\langle c \rangle_{arrest}$ at a given concentration. For the Newtonian systems, the values of $\langle c \rangle$ at long times exhibit a weak dependence on ϕ_A that precludes perfect collapse of the data at large values of $Y^*_{M,\phi}$. Below about $Y^*_{M,\phi} \approx 0.2$, the arrested structures consist almost entirely of un-yielded individual particles that are arrested immediately in their initial positions, so that $\langle c \rangle_{arrest}$ approaches 1 for $Y^*_{M,\phi} = 1$.

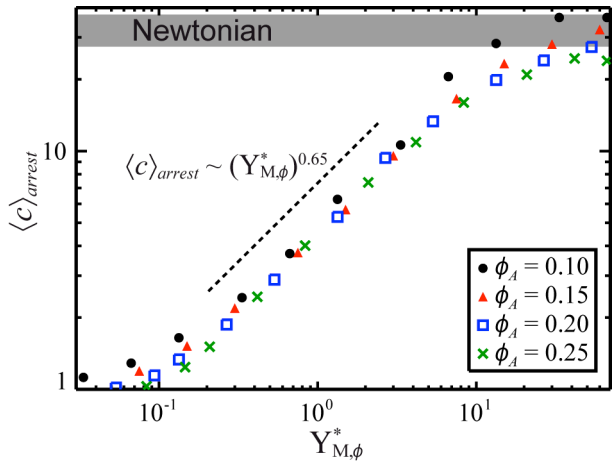

Figure 5. Average cluster size at structural arrest, $\langle c \rangle_{arrest}$, as a function of the concentration-scaled magnetic yield parameter, $Y^*_{M,\phi}$ (see eq 11). Data for four concentrations of magnetic particles collapse onto a universal power law over almost two orders of magnitude in $Y^*_{M,\phi}$. Below about $Y^*_{M,\phi} = 0.2$, the arrested structures consist primarily of individual particles, so that $\langle c \rangle_{arrest}$ approaches unity. The scaling begins to break down for $Y^*_{M,\phi}$ values greater than about 7, as Newtonian behavior is approached.

4. Conclusions

The chain structures formed when dispersions of polarizable particles are subjected to a uniform magnetic field provide the basis for a number of emerging and promising technologies involving multi-phase complex fluids, including magnetorheological suspensions[15] and lab-on-a-chip separation techniques.[16] More generally, field-directed assembly of magnetic colloids and nanoparticles has been exploited to design and engineer highly-ordered functional materials[34] with unique optical[12] or electrical[35] properties. In this letter, we have used particle-level simulations to investigate a new approach for mediating the field-induced assembly of dipolar particles via control of the non-Newtonian properties of the matrix fluid. Specifically, we have demonstrated the ability of the matrix fluid yield stress to arrest chain formation and growth at a critical point along the Newtonian trajectory. The magnetic yield parameter Y_M^* (eq 7), which characterizes the balance between inter-particle magnetic stresses and the matrix fluid yield stress, as well as the more general form $Y_{M,\phi}^* = Y_M^* \phi_A^2$ (eq 11) incorporating concentration variations, have been identified as the appropriate dimensionless groups that govern the structure and dynamics in these systems. This work addresses important questions in the field of magnetorheological (MR) suspensions regarding the nature of the field-induced microstructure when yield stress matrix fluids are used to prevent magnetic particle sedimentation.[19,20] Our observations indicate that for $Y_{M,\phi}^*$ values less than about 10, the matrix fluid yield stress will arrest chain growth and significantly decrease the size of clusters compared to the Newtonian case. Depending on the gap thickness in the rheometer or MR device, these truncated clusters will likely diminish or eliminate the gain in the yield stress anticipated upon application of the magnetic field. It is therefore desirable to operate yield-stress stabilized MR devices in the regime $Y_{M,\phi}^* \gg 10$, where the structures giving rise to the MR effect closely resemble those in Newtonian matrix fluids.

While the arrested structures demonstrated here represent states along the Newtonian trajectory, the effect of the matrix fluid yield stress to 'freeze' structures in place could be exploited in more exotic systems to assemble and stabilize more complex anisotropic particle structures with high degrees of order. As long as the inter-particle forces in the final structured states are insufficient to overcome the matrix fluid yield stress (a balance that could be characterized by dimensionless groups analogous to those used here), the assembled structures will be stable essentially indefinitely. If necessary, the structures can be adjusted subsequently by increasing the forces on particles as desired, or, alternatively, by decreasing the yield stress. This approach is not limited to magnetic assembly, but is straightforwardly extendable to systems with other types of particle interactions or external forces (e.g., electric fields, optical tweezers, etc.). It is even possible that different assembly techniques could be applied sequentially, with the yield stress matrix fluid trapping particles in place between steps,

allowing the complexity of achievable structures to be greatly expanded. Additionally, other types of non-Newtonian behavior in the matrix fluid could be similarly utilized to alter assembly. Though the task remains to confirm experimentally the behavior presented here, our results are physically reasonable and expected to be in at least qualitative agreement with experiments as long as the matrix fluid yield stress and inter-particle dipolar interactions are the dominant phenomena.

Acknowledgements

The authors thank Dr. Ramin Haghgooie for providing the initial version of the simulation code and for many helpful discussions. We additionally thank William Uspal for assistance in using computational facilities. Acknowledgement is made to the Donors of the American Chemical Society Petroleum Research Fund (ACS-PRF Grant No. 49956-ND9) for financial support.

Supporting Information

Movies of field-induced chain-formation for $\phi_A = 0.15$ at Y_M^* values of 6.7, 33, 67, and 133, as well as the Newtonian case $\left(\mathrm{Y}_\mathrm{M}^* \to \infty\right)$, out to dimensionless times of $\hat{t} = 16.7$, 167, 300, 800, and 2667, respectively; movies for $\phi_A = 0.15$ of a Newtonian system (black particles) overlaid with a system at $\mathrm{Y}_\mathrm{M}^* = 67$ (white particles) starting from the same initial condition out to dimensionless times of $\hat{t} = 6.7$ and $\hat{t} = 1667$; evolution of the average cluster size at $\mathrm{Y}_\mathrm{M}^* = 67$ starting from initial conditions corresponding to the arrested configurations at other values of Y_M^* for $\phi_A = 0.15$ (i.e., demonstration of history effects); evolution of the ensemble-averaged root mean square difference between particle positions in the Newtonian and yield stress system at $\phi_A = 0.15$ with dimensionless time re-scaled by the arrest time $\hat{t}_{arrest}$; section of a magnified image of Figure 4(A).

References

1. Whitesides, G. M.; Grzybowski, B., Self-assembly at all scales. *Science* **2002,** 295, 2418-2421.
2. Grzelczak, M.; Vermant, J.; Furst, E. M.; Liz-Marzan, L. M., Directed Self-Assembly of Nanoparticles. *ACS Nano* **2010,** 4, 3591-3605.
3. Xia, Y. N.; Gates, B.; Li, Z. Y., Self-assembly approaches to three-dimensional photonic

crystals. *Adv. Mater.* **2001,** 13, 409-413.
4. Gracias, D. H.; Tien, J.; Breen, T. L.; Hsu, C.; Whitesides, G. M., Forming electrical networks in three dimensions by self-assembly. *Science* **2000,** 289, 1170-1172.
5. Boncheva, M.; Andreev, S. A.; Mahadevan, L.; Winkleman, A.; Reichman, D. R.; Prentiss, M. G.; Whitesides, S.; Whitesides, G. M., Magnetic self-assembly of three-dimensional surfaces from planar sheets. *Proc. Natl. Acad. Sci. U.S.A.* **2005,** 102, 3924-3929.
6. Cui, H. G.; Webber, M. J.; Stupp, S. I., Self-Assembly of Peptide Amphiphiles: From Molecules to Nanostructures to Biomaterials. *Biopolymers* **2010,** 94, 1-18.
7. Zhang, S., Building from the bottom up. *Mater. Today* **2003,** 6, 20-27.
8. Glotzer, S. C.; Solomon, M. J., Anisotropy of building blocks and their assembly into complex structures. *Nat. Mater.* **2007,** 6, 557-562.
9. Yin, Y. D.; Lu, Y.; Gates, B.; Xia, Y. N., Template-assisted self-assembly: A practical route to complex aggregates of monodispersed colloids with well-defined sizes, shapes, and structures. *J. Am. Chem. Soc.* **2001,** 123, 8718-8729.
10. Park, S. J.; Lazarides, A. A.; Mirkin, C. A.; Letsinger, R. L., Directed assembly of periodic materials from protein and oligonucleotide-modified nanoparticle building blocks. *Angew. Chem.-Int. Edit.* **2001,** 40, 2909-2912.
11. Choi, J.; Rubner, M. F., Influence of the degree of ionization on weak polyelectrolyte multilayer assembly. *Macromolecules* **2005,** 38, 116-124.
12. Golosovsky, M.; Saado, Y.; Davidov, D., Self-assembly of floating magnetic particles into ordered structures: A promising route for the fabrication of tunable photonic band gap materials. *Appl. Phys. Lett.* **1999,** 75, 4168-4170.
13. Fermigier, M.; Gast, A. P., Structure evolution in a paramagnetic latex suspension. *J. Colloid Interface Sci.* **1992,** 154, 522-539.
14. Klingenberg, D. J., Magnetorheology: applications and challenges. *AIChE J.* **2001,** 47, 246-249.
15. de Vicente, J.; Klingenberg, D. J.; Hidalgo-Alvarez, R., Magnetorheological fluids: a review. *Soft Matter* **2011,** 7, 3701-3710.
16. Doyle, P. S.; Bibette, J.; Bancaud, A.; Viovy, J.-L., Self-assembled magnetic matrices for DNA separation chips. *Science* **2002,** 295, 2237.
17. Chhabra, R., *Bubbles, drops, and particles in non-Newtonian fluids*. CRC Press: Boca Raton, FL, 1993.
18. Feng, J.; Joseph, D. D., The motion of solid particles suspended in viscoelastic liquids under torsional shear. *J. Fluid Mech.* **1996,** 324, 199-222.
19. Rankin, P. J.; Horvath, A. T.; Klingenberg, D. J., Magnetorheology in viscoplastic media. *Rheol. Acta* **1999,** 38, 471-477.
20. Rich, J. P.; Doyle, P. S.; McKinley, G. H., Magnetorheology in an aging, yield stress matrix fluid. *Rheol. Acta* **2011**, (in review).
21. Haghgooie, R.; Doyle, P. S., Transition from two-dimensional to three-dimensional behavior in the self-assembly of magnetorheological fluids confined in thin slits. *Phys. Rev. E* **2007,** 75, 061406.
22. Haghgooie, R. Structure and Dynamics of Magnetorheological Fluids Confined in Microfluidic Devices. Massachusetts Institute of Technology, 2006.
23. Mohebi, M.; Jamasbi, N.; Liu, J., Simulation of the formation of nonequilibrium structures in magnetorheological fluids subject to an external magnetic field. *Phys. Rev. E* **1996,** 54, 5407-5413.
24. Zhang, H.; Widom, M., Field-induced forces in colloidal particle chains. *Phys. Rev. E* **1995,** 51, 2099-2103.
25. Flores, G. A.; Ivey, M. L.; Liu, J.; Mohebi, M.; Jamasbi, N. In Proceedings of the Fifth International Conference on ER Fluids, MR Suspensions, and Associated Technology, University of Sheffield, Sheffield, UK, 1995; Bullough, W., Ed. World Scientific, Singapore, 1996: p 140.
26. Heyes, D. M.; Melrose, J. R., Brownian dynamics simulations of model hard-sphere suspensions. *J. Non-Newton. Fluid Mech.* **1993,** 46, 1-28.
27. Pappas, Y.; Klingenberg, D. J., Simulations of magnetorheological suspensions in Poiseuille

flow. *Rheol. Acta* **2006,** 45, 621-629.
28. Beris, A. N.; Tsamopoulos, J. A.; Armstrong, R. C.; Brown, R. A., Creeping motion of a sphere through a Bingham plastic. *J. Fluid Mech.* **1985,** 158, 219-244.
29. Frenkel, D.; Smit, B., *Understanding Molecular Simulation: From Algorithms to Applications*. 2 ed.; Academic Press: Boston, MA, 2002.
30. Velev, O. D.; Bhatt, K. H., On-chip micromanipulation and assembly of colloidal particles by electric fields. *Soft Matter* **2006,** 2, 738-750.
31. Møller, P. C. F.; Fall, A.; Bonn, D., Origin of apparent viscosity in yield stress fluids below yielding. *Europhys. Lett.* **2009,** 87, 6.
32. Møller, P. C. F.; Fall, A.; Chikkadi, V.; Derks, D.; Bonn, D., An attempt to categorize yield stress fluid behaviour. *Philos. Trans. R. Soc. A-Math. Phys. Eng. Sci.* **2009,** 367, 5139-5155.
33. Roberts, G. P.; Barnes, H. A., New measurements of the flow-curves for Carbopol dispersions without slip artefacts. *Rheol. Acta* **2001,** 40, 499-503.
34. Ahniyaz, A.; Sakamoto, Y.; Bergstrom, L., Magnetic field-induced assembly of oriented superlattices from maghemite nanocubes. *Proc. Natl. Acad. Sci. U.S.A.* **2007,** 104, 17570-17574.
35. Tanase, M.; Silevitch, D. M.; Hultgren, A.; Bauer, L. A.; Searson, P. C.; Meyer, G. J.; Reich, D. H., Magnetic trapping and self-assembly of multicomponent nanowires. *J. Appl. Phys.* **2002,** 91, 8549-8551.